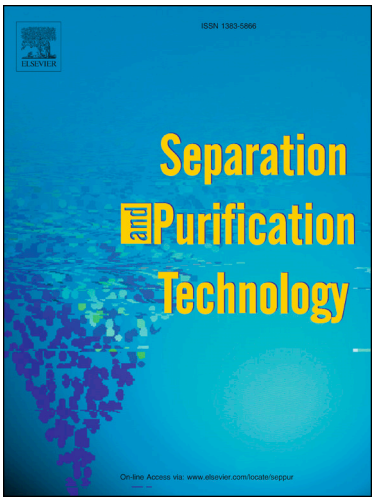


# Electrochemical water softening: influence of water composition on the precipitation behaviour

Ignacio Sanjuán, David Benavente, Eduardo Expósito, Vicente Montiel

PII: S1383-5866(18)33209-X
DOI: https://doi.org/10.1016/j.seppur.2018.10.044
Reference: SEPPUR 15031

To appear in: *Separation and Purification Technology*

Received Date: 13 September 2018
Revised Date: 19 October 2018
Accepted Date: 19 October 2018

Please cite this article as: I. Sanjuán, D. Benavente, E. Expósito, V. Montiel, Electrochemical water softening: influence of water composition on the precipitation behaviour, *Separation and Purification Technology* (2018), doi: https://doi.org/10.1016/j.seppur.2018.10.044

# Electrochemical water softening: influence of water composition on the precipitation behaviour

Ignacio Sanjuán[a], David Benavente[b], Eduardo Expósito[a], Vicente Montiel[a,*]

[a] *Grupo de Electroquímica Aplicada, Instituto Universitario de Electroquímica, Departamento de Química Física, Universidad de Alicante, Apdo. 99, Alicante 03080, Spain.*

[b] *Departamento de Ciencias de la Tierra y del Medio Ambiente, Universidad de Alicante, San Vicente del Raspeig, Alicante 03690, Spain.*

Submitted to: Separation and Purification Technology

* Corresponding author:

e-mail address: vicente.montiel@ua.es (V. Montiel)

Tel.: + 34 965903628

Fax: + 34 965903537

## Abstract

Hardness in membrane concentrates implies lower water recoveries in desalination. Electrochemical water softening is considered as a possible solution to control this hardness. This technique is based on the electrochemically forced precipitation of insoluble compounds of hardness ions onto the cathode surface. In this work we studied, in practical conditions, the effect of water composition on the technique efficiency and on the properties of the electroprecipitates. Experiments were conducted with a filter-press reactor and a 3D stainless steel wool cathode and for waters of a fixed hardness but varying the following composition parameters between them: alkalinity, Mg/Ca relationship and presence of an anti-scalant compound. Precipitates were fully characterised by SEM, XRD, TG-DTA and $N_2$ adsorption. Efficiency was measured in terms of hardness removal, demonstrating that the technique removes Ca more efficiently than Mg and that the presence of an anti-scalant does not alter the results. The properties of the electroprecipitates (morphology, texture, porosity and components) were related to water composition, evidencing its relevant effect. Geochemical modeling was realised to explain the electroprecipitation behaviour and why calcite, aragonite, vaterite and brucite are the only phases detected. This information contributes to the technique development, necessary for a future application in desalination practice.

*Keywords:* Electrochemical softening, hardness control, calcium carbonate, magnesium hydroxide, concentrate.

## 1. Introduction.

Usable fresh water resources are heterogeneously distributed around the world and they are currently becoming scarce [1]. Saline water represents almost the 98% of the entire global water and therefore sea or brackish water desalination may be a possible solution to this water problem. Membrane-based technologies like Reverse Osmosis (RO), Capacitive Deionisation (CDI) and Electrodialysis (ED) are available with this aim but the costs, due to the concentrate production, still have to be minimised in order to make the technology more competitive [2–6]

This is troublesome because the reduction of concentrates volume is limited by the high hardness degree of saline water (high amount of $Ca^{2+}$, $Mg^{2+}$, $SO_4^{2-}$ and $HCO_3^-$ ions). Several methods have been employed to control the hardness problem [7–12] but an interesting alternative is the electrochemical water softening (EWS) [13–15]. The technique EWS is an electrochemical method which consists of performing the electrolysis of hard waters (Fig. 1). As a result of the electrochemical water reduction occurring on the cathode, pH on the cathode vicinity augments forcing the precipitation of the insoluble compounds onto its surface and thus removing the scale-forming ions from the solution. EWS presents the advantages of the electrochemical techniques [16], such as environmental compatibility, and easy process control. Nevertheless, the application of this technique has been limited only to cooling towers [14] because it presents some technical limitations which makes the method less competitive: a high cathode area requirement and a limiting current density beyond which the precipitation rate remains unalterable [17,18]. Its application in membrane-based desalination needs then a major development in order to overcome these limitations and be cost-effective.

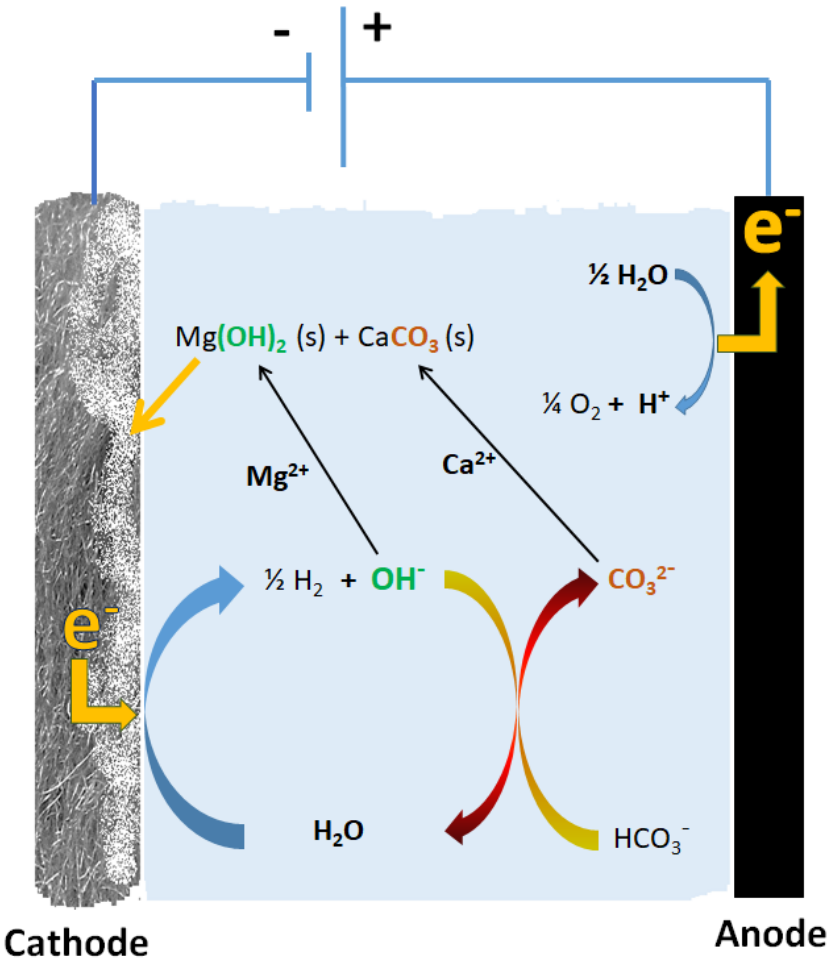


Fig. 1. Scheme of the electrochemical water softening process with accumulation of precipitate onto the cathode surface.

There are few works in literature dealing with the study of the electrochemical water softening method but it is well-known that the process efficiency and the type of precipitate strongly depends on various important parameters: electrode material and surface [19], operational conditions [13], and water composition [20]. The influence of the first two has been more studied and defined. In this sense, cathode is known to be highly relevant for the process, with stainless steel as the preferred choice because of the relationship efficiency to cost. Moreover, hydrodynamics is demonstrated to be another key parameter in this process with the conclusion that lower flow rates clearly give rise to better removals. Nevertheless, the effect of water composition on the electrochemical performance has not been studied in such detail, although it is known that some parameters like pH, ionic activities, and the presence of ionic/molecular species are determining for the features of the formed precipitate. From a fundamental point of view, more information about the scale is useful for the optimisation of the

technique. In this regard, a complete solid characterisation is needed: composition, morphology, crystal size, crystallinity, porosity, and texture. These precipitates properties will determine how the scale affects the cathode state and thus the technique efficiency [21].

For the study of electrochemically obtained precipitates (electroprecipitates), a vast variety of useful techniques are employed in literature: electrochemical impedance spectroscopy (EIS) [21], X-ray diffraction (XRD) [22], FTIR and RAMAN spectroscopy [23], scanning electron microscopy (SEM) [24], and transmission electron microscopy (TEM) [25]. Most of these studies are performed under controlled conditions: pure calco-carbonic waters, conventional electrochemical cells (glass and submerged impinging jet SIJ), potentiostatic mode and under the oxygen reduction domain [19,20,22,24,25]. Those conditions are far from a practical point of view in desalination, which necessarily involves electrochemical reactors, presence of magnesium and other ions, galvanostatic conditions, and water electroreduction. More works dealing with a full study of the precipitates in these practical conditions would be of great interest. Additionally, studies about the effect of different water compositions on the electrochemical technique efficiency are also scarce but interesting, since concentrates can be of varied nature.

In this work, we have evaluated the effect of different water compositions on the electrochemical softening in terms of hardness removal efficiency and solid features. Experiments have been conducted for waters of an always fixed hardness but altering, one at a time, the following composition parameters: alkalinity, Mg/Ca relationship, and an anti-scalant compound addition; specifically the sodium hexametaphosphate (HMP). The hardness removal efficiency is measured in all the cases and the solid fully characterised by SEM (morphology and texture), XRD (phases, crystallinity and crystal size), and thermogravimetry coupled to differential thermal analysis (TG-DTA). The porosity grade and microtexture of the solids were also studied by $N_2$ adsorption isotherms, which has not been applied to date to characterise this electroprecipitates. In addition, we modeled the evolution of the supersaturation index (SI), from the bulk solution to the cathode vicinity, with the aim to understand the behaviour of the electroprecipitation process. This study deals with a deeper understanding of the role of each component in the process, how they affect the efficiency and finally with the feasibility of each type of concentrate to be treated electrochemically. It should be noted that this study has been performed in practical conditions (electrochemical reactor,

galvanostatic mode, presence of different ions, and working with water electroreduction). A 3D stainless steel wool (SSW) has been introduced with a flow-through configuration since both presented good performance in the EWS, as already assessed in a previous work [26]. The information gathered after this work contributes to the technique development, in the interest for a future application in desalination practice.

## 2. Materials and methods

### 2.1. Chemicals reagents.

Magnesium sulphate heptahydrate, calcium chloride dihydrate, calcium nitrate tetrahydrate, sodium bicarbonate, sodium chloride, sodium sulphate anhydrous, sodium hexametaphosphate (HMP, $(NaPO_3)_6$) and ethylenediaminetetraacetic acid disodium salt dihydrate ($Na_2EDTA \cdot 2H_2O$) were purchased from Fluka at the ACS reagent grade (≥99%) and used without any further purification. Sulfuric ($H_2SO_4$) and hydrochloric (HCl) acid reagents were purchased from Sigma-Aldrich (95-97% and 35%, respectively). Ammonium chloride ($NH_4Cl$) was supplied by VWR Chemicals (99%), ammonia solution (35%) by Fluka and Eriochrome Black T indicator by Across Organics at the analytical reagent grade. Solutions employed in this work were always prepared with deionised water (3 MΩ·cm).

### 2.2. Composition of the feed water for the different experiments.

Working solutions were freshly prepared before each experiment, always with a fixed final hardness of 2300 - 2400 ppm as $CaCO_3$. Their composition is representative of common concentrates in membrane-based desalination of saline water. The preparation of the working solutions follows the same procedure described in [26]. The analytical determinations are also described in this previous work. Table ESI-1 displays the water composition data of the different experiments. Total hardness remained constant for all the experiments whereas the main influencing parameters of composition were separately varied for each experiment, as summarised in table 1. The standard experiment (Exp. S), the same used in the previous work, is used as reference. Exp. 1 solution has three times higher alkalinity than Exp. S whereas the Exp. 2 one has not $HCO_3^-$ in its composition. Exp. 3 solution has $Ca^{2+}$ and no $Mg^{2+}$ in its composition and Exp. 4 solution presents the opposite case. Exp. 5 solution incorporates an anti-scalant compound respect to the Exp. S: 0.2 mg $L^{-1}$ of HMP. HMP is widely used as

scale inhibitor by the membrane industry since concentrations below 5 mg $L^{-1}$ prevents the formation of calcium carbonate scale. The mechanism of HMP as scale inhibitor is based on its adsorption onto the active sites of the crystal growth. This increases the nucleation time and consequently prevents or delays the scale formation [27].

Table 1: summary of main parameters for the synthetic feed waters of each experiment.

| **Experiment** | **$H_o$ / mg $L^{-1}$ $CaCO_3$** | **Alcalinity / mg $L^{-1}$ $HCO_3^-$** | **Hardness ions** | **Precipitation inhibitor** |
|---|---|---|---|---|
| **1** | 2100 | 3300 | $Ca^{2+}$, $Mg^{2+}$, $HCO_3^-$ | - |
| **2** | 2300-2400 | 0 | $Ca^{2+}$, $Mg^{2+}$ | - |
| **3** | 2300-2400 | 1100 | $Ca^{2+}$, $HCO_3^-$ | - |
| **4** | 2300-2400 | 1100 | $Mg^{2+}$, $HCO_3^-$ | - |
| **5** | 2300-2400 | 1100 | $Ca^{2+}$, $Mg^{2+}$, $HCO_3^-$ | HMP |

### 2.3. Electrolytic system.

The electrolytic system and the optimum values of operation are the same used in the previous work [26]. For convenience of the reader, a scheme of the experimental system and another of the electrochemical reactor are shown in the electronic supporting information (ESI) with a detailed view of their elements (Figs. ESI-1 and ESI-2). A flow-through configuration (current parallel to the fluid flow) was used since it has been demonstrated to be more efficient for this process than the flow-by one (current perpendicular to the fluid flow).

### 2.4. Geochemical modeling.

PHREEQC code was used to simulate the evolution of the saturation index from the bulk to the electrode surface. The saturation index (SI) is defined as:

$$SI = \log\left(\frac{IAP}{K}\right) \quad (1)$$

where IAP is the ion activity product and K is the equilibrium constant. The saturation index determines whether the water is saturated (SI = 0), undersaturated (SI < 0), or supersaturated (SI > 0) with respect to the given mineral. Specific ion interaction theory is applied to estimate single-ion activity coefficients in electrolyte solutions, with an ionic strength values less than 2 mol $Kg^{-1}$ [28]. The variation of the equilibrium constant with temperature is here calculated using the Van't Hoff equation. The variation of pH from the bulk of the feed water to the vicinity of the electrode surface was simulated by adding different moles of NaOH in different steps using the methodology described in [29], in isothermal conditions, through REACTION keyword.

### 2.5. Precipitate characterisation.

Each cathode with the corresponding precipitate was collected after each experiment and rinsed slightly with distilled water to remove rests of soluble salts. Subsequently, it is dried overnight in oven at 45ºC. Temperature was set under the 60ºC in order to avoid crystal phase transitions.

Precipitate morphology and composition of the scale layer was carried out under scanning electron microscopy (SEM, HITACHI S-3000N microscope working at 20 kV with X-ray detector Bruker Xflash 3001 for microanalysis). For a better image resolution, samples were coated with a thin gold film produced with an SCD 04 high

vacuum evaporator for the morphological observations. The images were obtained for the precipitate onto the cathode surface while the rest of the techniques were applied on the powder extracted from the cathode.

The phase composition of precipitates was analysed by powder X-ray diffraction (XRD) on a Bruker D8-Advance diffractometer with mirror Goebel (non-planar samples) using the Cu Kα radiation and a setting of 40 kV and 40 mA. Data were collected and interpreted using the XPowder software package, which allows the nonlinear least squares quantitative analysis for the phases identified and global amorphous stuff, overall from the database records. The qualitative search-matching procedure was based on the ICDD-PDF2 database. Calcite, aragonite and brucite were identified and quantified by the JCPDS (Joint Committee on Diffraction Pattern standards). The unit cell information is: calcite (PDF standard 5-0586), with a = 4.989 Å, c=17.063 Å, γ=120º; crystal system: trigonal; space group R-3c, Nº 167. Aragonite (PDF standard 41-1475); with a=4.9623 Å, b=7.968 Å, c=5.7439 Å; crystal system: orthorhombic; Pmcn, Nº62. Vaterite (PDF standard 33-0268); with a=7.1473 Å, c=16.917 Å γ=120º; crystal system: hexagonal; P63/mmc, Nº=194. Brucite (PDF standard 7-0239); with a=3.147 Å, b=4.769 Å, γ=120º; crystal system: hexagonal; P-3m1, Nº=164. No other phases were found in the precipitates. It also takes into account a parameter that represents an approximate percentage of amorphous phases in the sample. The calculation of the global amorphous stuff considers that amorphous absorption contributes to the full-profile background. In this case, the analysis were obtained for the precipitate powder extracted from the cathode after the experiments.

Xpowder accomplishes microtexture analysis, including the classic Scherrer's method (1918). This method calculates the coherent domain size or the crystallite size of the precipitates, D(nm), from the reflection widths according to the Scherrer's formula:

$$D = \frac{K\,\lambda}{(B\cos\theta)} \tag{2}$$

where λ is the X-ray wavelength used (λ = 1.54 Å), K is the particle shape factor, which is a constant taken as 0.9, β the full width at half-maximum height (FWHM), and θ is the Braggs' angle (in rad) used in calculus. The most intensive reflection peaks of the samples were used in the line broadening analysis.

Textural performance was carried out by $N_2$ adsorption/desorption isotherms at -196ºC, which were acquired using an Autosorb-6 equipment (Quantachrome Instruments). Before the experiments, the samples were outgassed at 150ºC for 24 h with constant vacuum ($10^{-4}$ Torr). The specific BET surface ($S_{BET}$) and pore volumes were evaluated from the gas adsorption isotherms.

Thermal gravimetric analyses (TGA) coupled to differential analysis were realised using a model TGA/SDTA851and/SF/1100 (METTLER TOLEDO). The analyses were conducted under nitrogen atmosphere from 25 to 1000°C at a heating rate of 10°C $min^{-1}$ for all the materials.

### 2.6. Performance parameters.

The efficiency of hardness removal of the electrochemical technique was evaluated according to the parameter 'hardness conversion' (C, %). The C is given by the following equation:

$$C = \frac{H_o - H_f}{H_o} \cdot 100 \qquad (2)$$

where $H_o$ is the feed water hardness and $H_f$ is the steady state value of the treated water hardness, both expressed in mg $L^{-1}$ of $CaCO_3$.

The cell voltage ($V_{cell}$) and the cathode potential vs. AgCl/Ag (3.5 M KCl) standard reference electrode (CRISON) were also controlled. Experiments were carried out at least twice to check the reproducibility of the results. The temperature of the solutions was the laboratory temperature and it did not vary significantly during the experiments.

## 3. Results and discussion.

### 3.1. Effect of the water composition on the electrochemical softening efficiency.

The efficiency of EWS to remove hardness was investigated in terms of water composition. The C was calculated for each one of the experiments described in Table 1 with comparative purposes. The results of the experiments are summarised in Fig. 2.

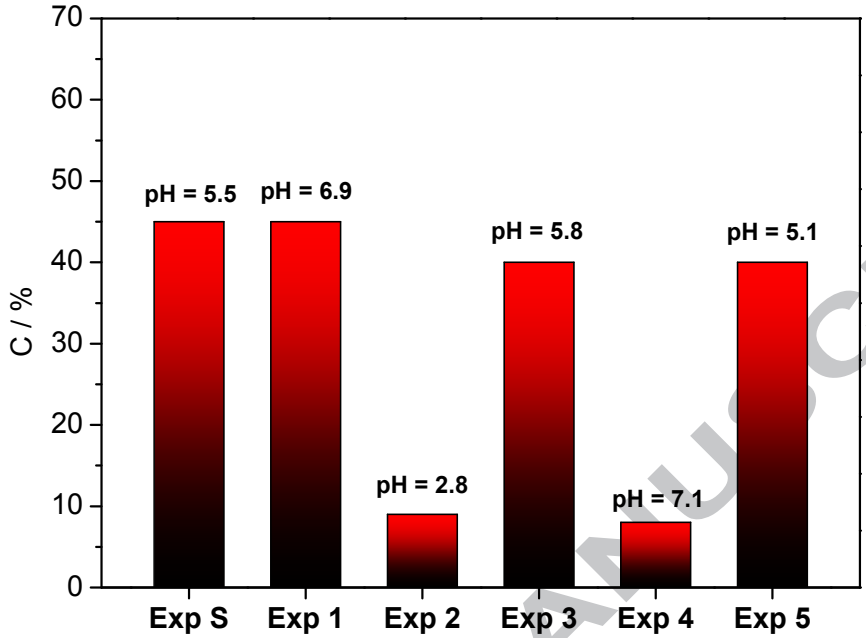


Fig. 2. Hardness conversion for each performed experiments. Above the corresponding bar is set the pH of the treated water in the steady state.

As we can see, the C obtained for Exp. 1 (Higher alkalinity), 3 (Only $Ca^{2+}$) and 5 (with HMP) is similar to the obtained for Exp. S. The C for Exp. 2 and 4 is similar between them but up to 35 percent points lower than for the rest of the experiments. Regarding the pH, it differs among the experiments. For Exp. 3 and 5 the pH is slightly acid (around 5) like in the case of Exp. S but, in the other cases, the final pH of the treated water changes. For Exp. 1 the solution is strongly buffered by the high concentration of $HCO_3^-$ and pH remains close to the neutrality whereas for Exp. 2 the opposite occurs. In the case of Exp. 4, the amount of $HCO_3^-$ is enough to buffer the solution since the process here is not efficient.

Regarding the cathode potential and the $V_{cell}$, Fig. ESI-3 displays the plot of these values with time for every experiment. It can be seen that both parameters remain practically constant during the experiment in all cases. Table ESI-2 shows the values of average $V_{cell}$ and cathode potential for each experiment and it can be seen that there are not significant differences in the values obtained for the different experiments. This could be attributed to the high cathodic area provided by the 3D SSW, which would require long-term experiments to be sufficiently covered by the scale. Due to

differences in the electrical conductivity of the solutions, cathodic potential values give better information than $V_{cell}$ about the effect of the electroprecipitates on the cathodic surface state, as it will be commented below.

Water composition is clearly of vital importance for the EWS efficiency. An excess of $HCO_3^-$ (Exp. 1) may not be useful since there is not any enhancement in efficiency and the Langelier index gets higher (higher alkalinity). On the contrary, an absence of $HCO_3^-$ (Exp. 2) leads to a very low efficiency and a noticeably pH decrease. It could be also concluded that $Ca^{2+}$ is removed more efficiently than $Mg^{2+}$ by the method (Exp. 3 and Exp.4). The EWS is more efficient for concentrates with Ca concentrations higher than Mg. This issue should be taken into account since the concentrate to treat can come from seawater or brackish water, in which the Ca/Mg ratio is different. Nonetheless, there is not any clear relationship between efficiency and the different kind of electroprecipitates since Exp. S, 1, 3, 5 present similar C. Only differences between Ca and Mg compounds have been observed. Finally, we also demonstrated that presence of an anti-scalant compound (Exp. 5), in this case HMP, does not affect the efficiency, at least in concentrations commonly used in desalination practice (0.2 mg $L^{-1}$ of HMP). Although an anti-scalant compound diminishes the rate of a homogeneous precipitation, the high alkaline environment / high supersaturation around the cathode vicinity forces the precipitation hindering the HMP effect.

### 3.2. Effect of water composition on the morphology of the obtained electroprecipitate.

As already mentioned, the morphology and texture of precipitates have relevancy on the electrochemical process. Fig. 3 shows the SEM images for the electroprecipitates obtained on the SSW cathode, for every experiment. The habit and size of crystals are very variable between different experiments, due to the formation of different phases and/or polymorphs.

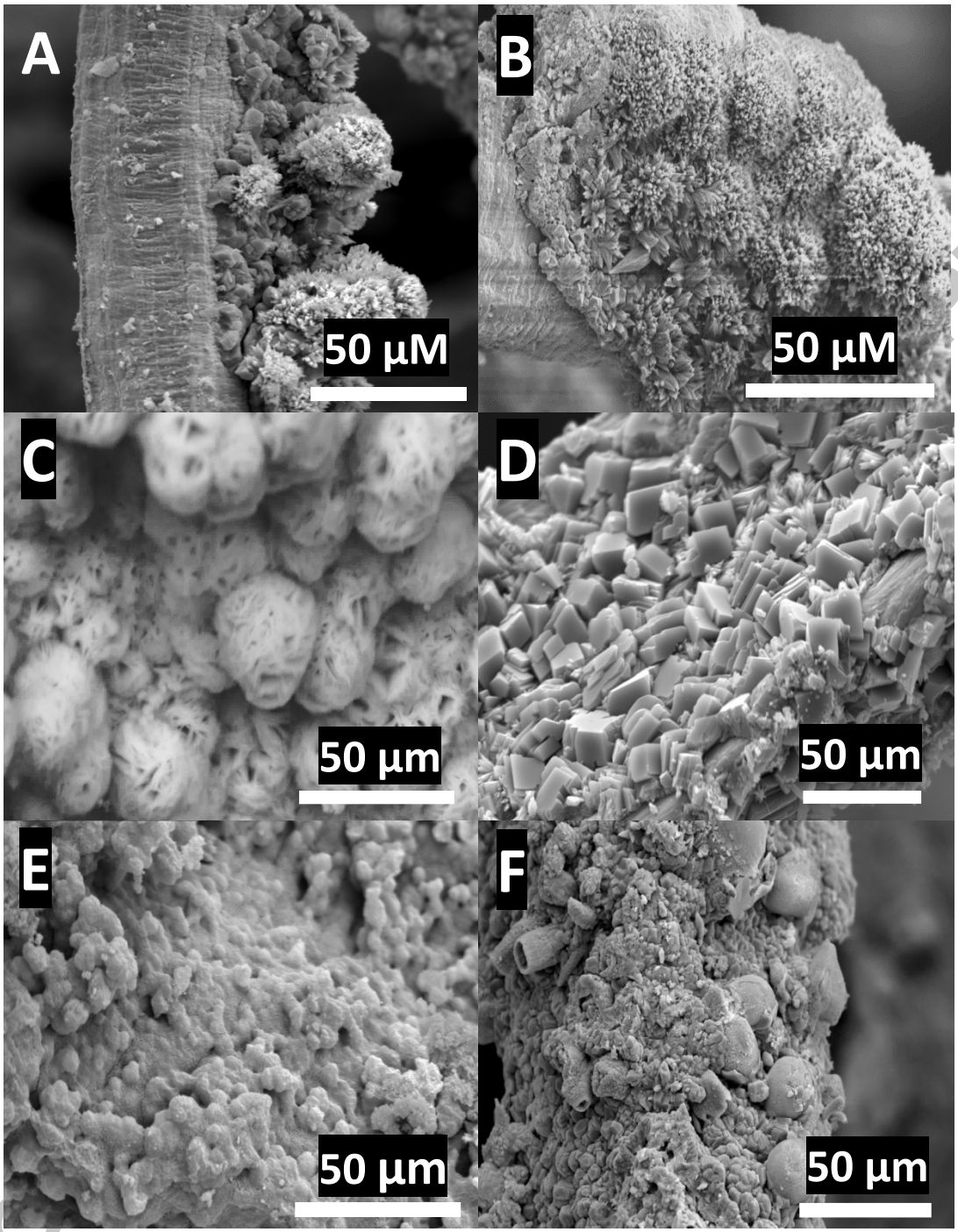


Fig. 3. SEM micrographs of the stainless steel wool cathode with electroprecipitate. Each micrograph corresponds to a different experiment: A) Exp. S (standard), B) Exp. 1 (higher alkalinity), C) Exp. 2 (nule alkalinity), D) Exp. 3 (only $Ca^{2+}$), E) Exp. 4 (only $Mg^{2+}$), F) Exp. 5 (addition of 0.2 mg $L^{-1}$ sodium hexametaphosphate).

For Exp. S (Fig. 3A), three main crystal forms can be distinguished: trigonal shape crystals, shrubs of thin needles and rough-surfaced spherulites, as already seen in the previous work [26]. The alkalinity showed a relevant role for the solid formation since in Fig. 2B only shrubs of thin needles are observed. In this case alkalinity is three times higher (Exp. 1) than in Exp. S, so the SI by $HCO_3^-$ is, and this leads to a faster

crystallization which forces the growth of needle-shaped crystals preferentially. Contrarily, the precipitate after Exp. 2 (absence of $HCO_3^-$) consisted of only big spheres with a perceptible grade of porosity (Fig. 3C). Regarding Fig. 4D, only trigonal crystals were observed. Absence of $Mg^{2+}$ in solution (Exp. 3) allows $Ca^{2+}$ compounds precipitate only as trigonal crystals. $Mg^{2+}$ may be responsible of the precipitation of the needles form. Otherwise, when only $Mg^{2+}$ is in solution (Exp. 4), precipitate is composed of spherulites (Fig. 3E). Finally, the addition of 0.2 mg $L^{-1}$of HMP (Exp. 5) produces a loss of the precipitate morphology compared to Exp. S, as can be seen in Fig. 3F. Big agglomerations and volcano-like forms are clearly detected and randomly distributed. This fact was already verified in the previous work. Results report that species present in solution have a relevant effect on texture, size and morphology of the formed crystals.

### 3.3. Effect of water composition on the crystalline properties of the formed electroprecipitate.

Precipitates were identified and quantified by XRD. The XRD pattern for the electroprecipitate powdered is shown in Fig. 4, for all the experiments. Found phases vary according to the feed water composition, as expected, although the only phases detected in general were calcite ($CaCO_3$), aragonite ($CaCO_3$), brucite ($Mg(OH)_2$) and vaterite ($CaCO_3$). No other possible phases were found with XRD, as magnesite ($MgCO_3$), dolomite ($CaMg(CO_3)_2$), magnesian calcites ($Ca_{1-X}Mg_xCO_3$), portlandite ($Ca(OH)_2$), nesquehonite ($MgCO_3 \cdot 3H_2O$) or calcium sulfates phases (gypsum, $CaSO_4 \cdot 2H_2O$, and anhydrite, $CaSO_4$). The identified phases and their quantification are described in Table 2. All the experiments, with the exception of Exp. 3, contain certain amount of an amorphous phase.

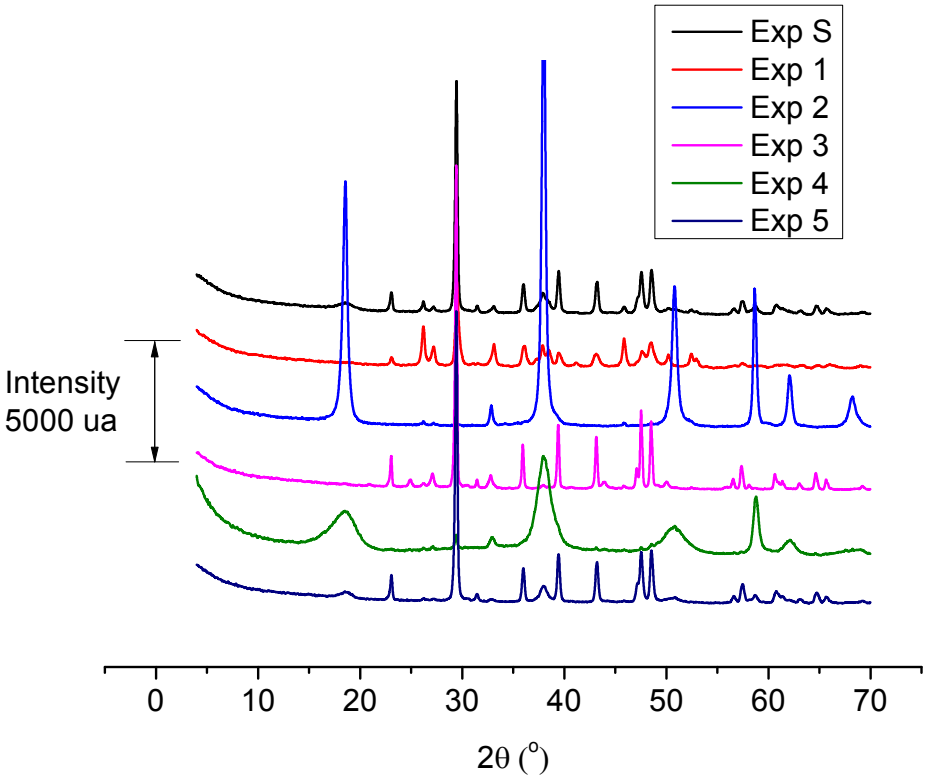


Fig. 4. Powder XRD diffractogram registered for the powder obtained from the electroprecipitate on the cathode, for the different experiments. The XRD diffractograms are arranged in an orderly way from the Exp. S at the top to the Exp. 5 at the bottom, as shown in the legend.

Table 2. Data of crystal phases identification and quantification obtained by XRD technique.

| **% Phase →** Experiment ↓ | **Calcite** | **Aragonite** | **Vaterite** | **Brucite** | **Amorphous** |
|---|---|---|---|---|---|
| S | 81 | 8 | n.d. | 6 | 5 |
| 1 | 47 | 42 | n.d. | n.d. | 11 |
| 2 | n.d. | n.d. | n.d. | 93 | 7 |
| 3 | 87 | 2 | 7 | n.d. | n.d. |
| 4 | n.d. | n.d. | n.d. | 79 | 21 |
| 5 | 88 | 2 | n.d. | 5 | 5 |

***n.d. - no detected***

For the Exp. S three phases were detected: calcite, aragonite and brucite; being calcite the most abundant. When the alkalinity is three times higher (Exp. 1), no precipitated brucite was detected while the amount of aragonite increases considerably. Also in this case, the amount of detected amorphous stuff is higher respect to the Exp. S. Otherwise, the lack of $HCO_3^-$ in solution (Exp. 2) gave rise to the precipitation of only brucite, and any kind of $Ca(OH)_2$ was precipitated in the conditions provided by the electrochemical technique. For the experiment without $Mg^{2+}$ (Exp. 3), brucite is not observed and the calcite/aragonite ratio is similar than in the case of Exp. S. Interestingly the phase vaterite was here detected. The presence of $SO_4^{2-}$ may promote the stabilisation of this unstable polymorph [30]. For the case of Exp. 4 (only $Mg^{2+}$) logically only brucite is detected, in a 79% as a crystalline compound and a 21% as an amorphous phase. Exp. 1 and 4 present more amorphous compounds than the rest of the experiments. Finally, there is not any significant difference between the Exp. 5 (with HMP) and the Exp. S (without HMP) except that in the last case the calcite/aragonite ratio is slightly higher.

Water composition therefore plays an important role in the compounds finally precipitated. A higher concentrations leads to a faster precipitation and thus aragonite precipitates rather than calcite by kinetic reasons and more amount of global amorphous stuff is formed as well. The absence of $HCO_3^-$ avoids the precipitation of any form of Ca compounds. Although calcite is the most thermodynamically stable $CaCO_3$ form, the presence of $Mg^{2+}$ in solution promotes the formation of aragonite [31,32] and additionally diminishes the formation of trigonal shaped crystals. Otherwise, its absence gives rise to the formation of a clear abundance of those trigonal crystals and allows the detection of vaterite. $Mg^{2+}$ inhibits the formation of vaterite or forces its transformation into aragonite, since vaterite is an unstable polymorph [25,32,33]. It is also worth noting that brucite has clearly more amorphous forms than carbonates (this matches with SEM observations). When brucite is present in the precipitates, there is a high background distributed in a wide range of XRD pattern, which is estimated by the percentage of global amorphous stuffs. Finally, it can be checked that presence of HMP in solution does not affect the formation of the crystal phases compared to the standard experiment in spite of the morphology is clearly altered, as seen by SEM in the previous section. Comparing the SEM and the XRD analyses and according to typical forms of phases, we can corroborate that the trigonal shape crystals observed in Exp. 1 and 3 can be

attributed to the calcite polymorph ($CaCO_3$) [19,22], the needles may correspond to the aragonite form ($CaCO_3$) [21,25] and the spherulites could be assigned to the formation of brucite ($Mg(OH_2)$) [13]. Ca and Mg are separately eliminated in different pure compounds (perfect match between d-spacing of the phases in the XRD pattern and their standards).

Nevertheless, the quantification of precipitate components by XRD is not accurate enough. Consequently, TG-DTA measurements (Fig. ESI-4) were performed in order to complete the information obtained by XRD. By this technique, the total amount of $Mg(OH)_2$ and $CaCO_3$ was calculated according to the mass loss of the precipitate by their thermic decomposition at 360 and 700ºC, respectively. The corresponding results are presented in table 3 and they correspond well with the obtained by XRD, confirming the validity of the composition analysis. The only little discrepancy is the amount of $Mg(OH)_2$ in Exp. S, 1 and 5. As a result of the comparison between the numbers of XRD and TG-DTA, discrepancies can be attributed to the formation of amorphous forms of $Mg(OH)_2$, which are not accurately measured by XRD.

Table 3. Quantification of Ca and Mg insoluble compounds in the precipitate by TG-DTA technique.

| **% Compound →** Experiment ↓ | $CaCO_3$ | $Mg(OH)_2$ |
|---|---|---|
| S | 78 | 22 |
| 1 | 89 | 11 |
| 2 | n.d. | 100 |
| 3 | 100 | n.d. |
| 4 | n.d. | 100 |
| 5 | 78 | 22 |

***n.d. - no detected***

Crystallinity properties of precipitates are also here estimated from the crystallite size and amorphous components. For XRD, the smallest crystallite size cause obvious broadening of the XRD peaks due to crystalline imperfections and other structural features. Scherrer's formula (equation 2) highlights the inverse relationship between crystallite size, D, and peak width, FWHM. Amorphous solids do not possess that periodicity and atoms are randomly distributed in 3D space. X-rays will be scattered in

many directions leading to a large bump and high background distributed in a wide range of diffraction angles (2θ) instead of high intensity narrower peaks. Crystalline precipitates cause a discrete X-ray diffraction pattern with high intensity peaks whereas amorphous precipitates act as a material with a diffuse X-ray diffraction pattern. As a result, when amorphous solids are present in a crystalline material, its XRD pattern will be a mixture of both. Table 4 summarises the values of the half-maximum height (FWHM) and the crystalline size (D) using the Scherrer's formula on the main reflections peaks for calcite, aragonite, vaterite and brucite. Values for aragonite in Exp. 3 and 5 do not appear because the corresponding XRD peaks had little height to carry out the calculus.

Table 4. Data of width and crystal size calculated (Equation 2) for the main reflection peaks of all the crystal phases and experiments.

| **FWHM (º)** | Calcite | Aragonite | Vaterite | Brucite |
|---|---|---|---|---|
| Experiment ↓ | (104) | (111) | (114) | (101) |
| S | 0.221 | 0.204 | n.d. | 0.873 |
| 1 | 0.291 | 0.274 | n.d. | n.d. |
| 2 | n.d. | n.d. | n.d. | 0.384 |
| 3 | 0.143 | - | 0.33 | n.d. |
| 4 | n.d. | n.d. | n.d. | 1.589 |
| 5 | 0.193 | - | n.d. | 0.728 |

| **Scherrer (nm)** | Calcite | Aragonite | Vaterite | brucite |
|---|---|---|---|---|
| Experiment ↓ | (104) | (111) | (114) | (101) |
| S | 35 | 34 | n.d. | 9 |
| 1 | 27 | 27 | n.d. | n.d. |
| 2 | n.d. | n.d. | n.d. | 22 |
| 3 | 48 | - | 23 | n.d. |
| 4 | n.d. | n.d. | n.d. | 6 |
| 5 | 39 | - | n.d. | 12 |

***n.d. - no detected***

Average crystallite sizes of carbonates and brucites changes in each experiment, which means water composition affects the crystalline properties of the formed scale. Within the same experiment, calcite and aragonite present similar crystallite sizes in spite of having different morphology (SEM). Higher concentrations, by the high amount of $HCO_3^-$ (Exp. S vs 1) or $Mg^{2+}$ (Exp. 2 vs 4), mean rapid nucleation and thus it gives

rise to a smaller crystal sizes. Moreover, Mg compounds have less crystallinity properties and they are responsible for amorphous phases formation [34]. $Mg^{2+}$ also affects to the crystallite size of carbonates since Exp. 3 (only $Ca^{2+}$) shows the narrowest peaks and thus the biggest crystals. Remarkably, the addition of HMP does not significantly alter the size of the crystals formed.

### 3.4. Effect of water composition on the porosity and microtexture of the solids.

The porosity of the precipitate is crucial for this process because it affects the cathode potential and thus the energy consumption. All the solids formed during the process are totally insulating and their precipitation on the cathode means the active surface is being blocked, which leads to higher cathode potentials and consequent higher energy consumptions. A less porous solid is expected to block the cathode in a higher degree.

Table 5 presents the results of the analysis of the $N_2$ isotherms (Fig. ESI-5) obtained for each precipitate. Solid from Exp. 3 (only $Ca^{2+}$) has the lowest surface area and the lowest porosity. This fits well with SEM since observed trigonal crystals seem to be little porous and the scale looks quite compact. Contrarily, Exp. 4 shows the most porous solid with highest surface area (significantly higher than the rest). If we compare the Exp. 2 and 4; where only brucite is present, it is evidenced that solids of Exp. 4 have much more area than the Exp. 2 ones. Higher porosity and surface area for Exp. 4 is expected to be caused by the formation of smaller brucite crystals (clearly seen by SEM) and a higher amount of amorphous stuff.

Comparing the results of porosity (Table 5) with the data of average cathodic potentials (Table ESI-2), we can conclude that there is not a clear relationship between both. For example, electroprecipitate of Exp. 4 is the most porous but giving rise to the highest cathode potential whereas electroprecipitate of Exp. 3 gives rise to the lowest cathode potential being the least porous. It could be expected, at first, that a more porous precipitate would lead to a lower cathode potential. In general, this kind of insoluble compounds are poorly porous solids and their influence on the cathode potential should be related to the way with the particles are compacted/adhered onto the cathode surface more than with the porosity of the material itself.

Table 5. Data of $N_2$ BET surface area and total pore volume determinated at -196ºC for the solids of each experiment.

| Experiment | BET surface area / $m^2\ g^{-1}$ | Total pore volume / $cm^3\ g^{-1}$ |
|---|---|---|
| S | 6.33 | $1.57 \cdot 10^{-2}$ ( $\phi_{pore} < 51$ nm) |
| 1 | 12.78 | $4.23 \cdot 10^{-2}$ ( $\phi_{pore} < 49$ nm) |
| 2 | 19.26 | $8.29 \cdot 10^{-2}$ ( $\phi_{pore} < 48$ nm) |
| 3 | 2.76 | $7.90 \cdot 10^{-3}$ ( $\phi_{pore} < 51$ nm) |
| 4 | 60.93 | $2.45 \cdot 10^{-1}$ ( $\phi_{pore} < 46$ nm) |
| 5 | 10.99 | $4.50 \cdot 10^{-2}$ ( $\phi_{pore} < 52$ nm) |

Also, we can conclude that brucite is a more porous phase than carbonates and thus the presence of Mg in solution will give rise to a more porous precipitate. Comparing the sequence Exp. S, 1, 3 and 5, it can be also concluded that aragonite is a $CaCO_3$ phase more porous than calcite and with more surface area [21,24,35]. Higher alkalinities provide more porous precipitates since aragonite is the most predominant form in this case. In addition, faster precipitations by a high concentration of some of the precursors will give rise to a smaller crystals and consequently higher porosity. Lack of alkalinity avoids the precipitation of Ca compounds, so finally leads to a more porous precipitate as well. Finally, addition of HMP give rise to a more porous precipitate and with more surface area in spite of having the same composition and properties, according to XRD and TG-DTA. It is in agreement with SEM observations where for the Exp. 5 the precipitate had lost the morphology of Exp. S and volcano-like forms appeared. As a conclusion, it can be stated that the water composition strongly affects the porosity of the final precipitates and therefore to the electrochemical performance indirectly. The presence of $Mg^{2+}$ results in a more porous precipitate as well as high alkalinities or the presence of HMP does. Nevertheless, the porosity degree does not correlate with cathode potentials as it could be expected. The solid with higher amount of calcite (the least porous polymorph) presents the lowest average cathode potential value. In this case, the compactness of the solids on the cathode surface must be more important for the cathode block than the porosity of the material itself. As already said, long-term experiments would be of great interest for a deeper study of the cathode block since the high cathodic area provided by the 3D SSW would require experiments of longer duration to achieve a significant cathode obstruction.

### 3.5. Geochemical modeling.

PHREEQC code was used to simulate the evolution of SI from the bulk to the electrode surface in order to better understand the behaviour observed with the previous techniques. In Fig. 5, the values of calculated SI are plotted versus pH, for all the possible compounds in each case. SI varies from the bulk solution to the cathode vicinity, where the precipitation process takes place. It is important to know the SI of the most likely products precipitating in the cathode vicinity and this will depend directly or indirectly on the interfacial pH (local pH in the cathode vicinity). In this regard, a scarce number of works deals with the theoretical calculation and experimental measurement of the interfacial pH during oxygen reduction [36,37]. In both cases, a well-defined hydrodynamics conditions are necessary. In the case of this work, the measurement or calculation of this interfacial pH is extremely complicated because the hydrodynamic conditions are not well-defined, since an electrochemical reactor and a 3D electrode are employed. Therefore, the interfacial pH was roughly estimated considering the following assumptions: (i) interfacial pH is considered as the pH in the layer of solution in contact with the cathode, which is not affected by convection (Nernst diffusion layer) and where the electrochemical and precipitation reactions are supposed to take place. (ii) The volume of solution of this layer was estimated by the cathodic area (around 225 $cm^2$ [26]) and the effective thickness of the layer, which is supposed to be around 0.011 cm, taking into account the hydrodynamic conditions of low flow rate used in this work [38]. (iii) Once estimated this volume, the moles of $OH^-$ generated per second (intensity current), the concentration of $HCO_3^-$ and its buffering capacity; the interfacial pH is assumed to be close to the value 10. This value is highlighted in Fig. 5 with a vertical orange dashed line.

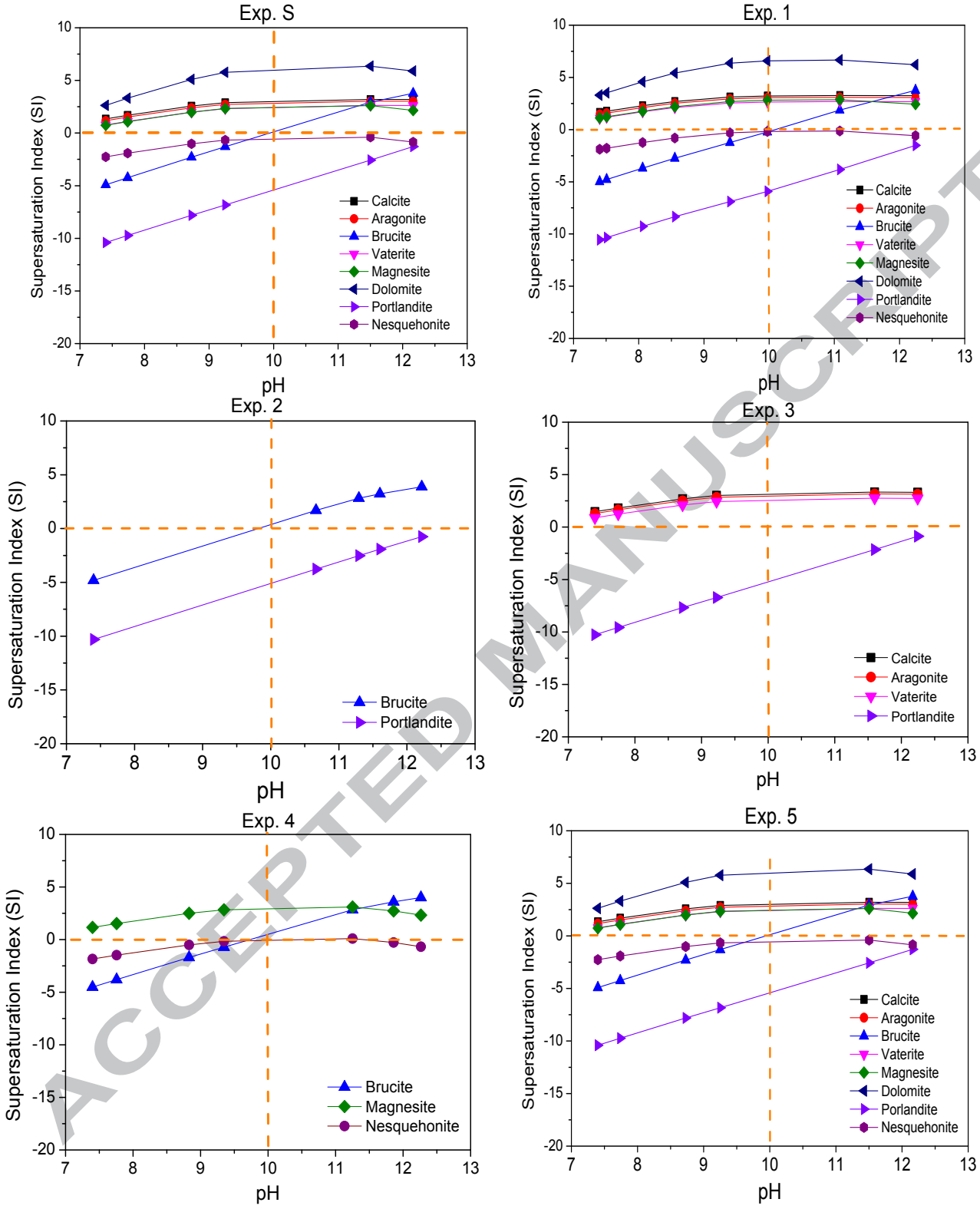


Fig. 5. Plot of SI calculated by PHREEQC code versus pH, for all the experiments and all the probable compounds in each case. Vertical orange dashed line highlights the estimated pH in the reaction layer close to the cathode and horizontal orange dashed line marks the SI value of 0 (saturation). SI > 0 = supersaturated, SI < 0 = undersaturated.

Fig. 5 reveals that SI of minerals generally increases as pH increases (interfacial pH is quite higher than bulk pH). Carbonates and brucite reach important SI values, which may cross the supersolubility line (spontaneous crystallisation is probable) and this may explain why they are the main phases observed. Calcite, aragonite, vaterite and dolomite are supersaturated in both the bulk solution and the vicinity of the cathode, in all the experiments where they are possible to be formed. Calcite is the most stable phase of the calcium carbonate phases at room temperature. However, aragonite is also observed in Exp. S, 1, 3 and 5 as well as vaterite in Exp. 3. Presence of these $CaCO_3$ metastable phases may be explained because both are supersatured from the bulk to the cathode and they are easier to nucleate. According to Gay-Lussac-Ostwald or Ostwald step rule, the nucleation of a more soluble phase (such as amorphous or a metastable phase) is kinetically favoured over less soluble analogues (such as calcite) because of the lower interfacial energy (and thus lower nucleation energy) between minerals and solution. Hence, when the supersaturation of the solution is sufficiently high, the metastable mineral may have a higher rate of precipitation. In other words, the solid that reduces supersaturation faster will be formed in first place. Although the bulk solution is supersaturated for these compounds, they do not precipitate because their SI must not be high enough to avoid kinetic limitations. It should be noted that homogeneous precipitation requires higher supersaturation degrees than the heterogeneous one [13]. Moreover, brucite is always undersaturated in the bulk of the feed water but seems to reach a supersaturation level at high pH, like the interfacial one. Its SI is higher in Exp. 2 and 4 than in Exp. S, 1 and 5 because in Exp. 2 there is not $HCO_3^-$ to reach the $OH^-$ generated on the cathode and in Exp. 4 the concentration of Mg is higher. Brucite undergoes the strongest variation index at pH from 7 to 12, being nearly linear, with a SI/pH rate of 1.9. Thus, in the hundred micrometers close to the cathode, brucite reaches high supersaturations and suffers rapid nucleation that may form nonequilibrium with low crystallinity and/or amorphous phases. In the brucite precipitation, supersaturation is important but supersaturarion rate is even more critical. SI for brucite in the conditions near of the cathode surface is lower than the SI for calcite and aragonite and this fact can explain why the hardness removal efficiency is lower for the experiments in which only Mg is removed. Dolomite and magnesite are supersaturated in the feed waters, although their precipitations are kinetically hindered. In most of these phases, kinetic barriers (not thermodynamic) can provide ultimate drivers in their precipitation. Dolomite precipitation has been widely studied in natural systems (named as dolomite

problem) and the disparity between its abundance in the geologic record and its paucity in modern environments despite being supersaturated is still in controversy [28]. Power et al. (2017) [39] point out that at ambient pressure and low temperatures (< 60°C), magnesite precipitation is kinetically inhibited due to the strong hydration of $Mg^{2+}$ ions in solution. Otherwise, portlandite is totally unsaturated in both the bulk solution and the cathode surface and consequently, this compound cannot precipitate in any experiment. The same occurs for nesquehonite. Influence of the water composition is key for the precipitation behaviour and the final electroprecipitate composition.

## 4. Conclusions.

In this work, the electrochemical water softening has been investigated to remove hardness from waters with different compositions. The effect of water composition, on the technique efficiency and on the properties of the electroprecipitate formed, has been evaluated in practical conditions. Experiments have been conducted with a filter-press reactor and a 3D stainless steel wool cathode, for waters of a fixed hardness but varying the following composition parameters: alkalinity, Mg/Ca relationship, and presence of an anti-scalant compound. Results demonstrated that water composition has a relevant effect on the technique efficiency. For instance, the technique removes Ca more efficiently than Mg and the presence of an anti-scalant compound does not alter the results. However, certain level of alkalinity ($HCO_3^-$) is necessary because Ca only is removed as carbonate. Electrochemical softening technique may be adequate to remove hardness from waters whose composition is similar to concentrates with high hardness degree and high Ca/Mg ratio. There is not any relationship between the hardness removal efficiency and the different kind of precipitates, only differences between Ca and Mg compounds, at least at the duration of the experiment. Also, water composition has been proved to strongly affect the properties of the solid electroprecipitated after a full characterisation of them by SEM, XRD, TG-DTA and $N_2$ adsorption, for all the experiments. The presence or ausence of some of the reactants ions will determine the composition, the form, the crystallinity and cristal size, and the porosity of the formed solids. Moreover, high amount of some reactant ion (high SI values) will also influence these properties. On the other hand, presence of anti-scalant HMP only affects to the morphology and consequently to the porosity of the precipitate. The importance of this lies on the influence of the electroprecipitate on the state of the cathode will have to do with the cathode potential

(energy consumption) and the adherence of the precipitates. The adherence will have consequences in the performance of the cathode cleaning process. The electroprecipitation behaviour has been explained by geochemical modeling and this confirms why calcite, aragonite, vaterite and brucite are the only phases detected and the conclusion was that although other phases are also supersaturated close to the electrode, due to kinetic limitations they are not able to precipitate. The information gathered after this work contributes to the technique development, looking for overcoming the technique limitations which avoid its application in desalination practice.

**Acknowledgements.**

I. Sanjuán would like to acknowledge the Ph.D. fellowship granted and the material and human resources provided by the University of Alicante and the company Aguas de Valencia, S.A.

**References.**

[1] UNESCO, World Water Development Report Volume 4: Managing Water under Uncertainty and Risk, 2012. doi:10.1608/FRJ-3.1.2.

[2] F. a. AlMarzooqi, A. a. Al Ghaferi, I. Saadat, N. Hilal, Application of Capacitive Deionisation in water desalination: A review, Desalination. 342 (2014) 3–15. doi:10.1016/j.desal.2014.02.031.

[3] S. Kim, C. Kim, J. Lee, S. Kim, J. Lee, J. Kim, et al., Hybrid Electrochemical Desalination System Combined with an Oxidation Process, ACS Sustainable Chemistry and Engineering. 6 (2018) 1620–1626. doi:10.1021/acssuschemeng.7b02789.

[4] P. Taylor, S. Lee, Y. Kim, A.S. Kim, S. Hong, Evaluation of membrane-based desalting processes for RO brine treatment, Desalination and Water Treatment. (2015) 37–41. doi:10.1080/19443994.2015.1030120.

[5] G. Amy, N. Ghaffour, Z. Li, L. Francis, R.V. Linares, T. Missimer, et al., Membrane-based seawater desalination: Present and future prospects, Desalination. 401 (2016) 16–21. doi:10.1016/j.desal.2016.10.002.

[6] AFFA, Introduction to desalination technologies in Australia, 2002. http://scholar.google.com/scholar?hl=en&btnG=Search&q=intitle:Introduction+to+Desalination+Technologies+in+Australia#0.

[7] N.V. Malanova, V.V. Korobochkin, V.I. Kosintsev, The Application of Ammonium Hydroxide and Sodium Hydroxide for Reagent Softening of Water, Procedia Chemistry. 10 (2014) 162–167. doi:10.1016/j.proche.2014.10.028.

[8] V.B. Obraztsov, E.D. Rubl'ova, O.S. Baskevych, Influence of the Scaling Inhibitor on the Phase Composition, Morphology, and Sedimentation Properties of CaCO3 Deposits, Materials Science. 51 (2016) 652–658. doi:10.1007/s11003-

016-9887-3.

[9] X. Li, H. Shemer, D. Hasson, R. Semiat, Characterization of the effectiveness of anti-scalants in suppressing scale deposition on a heated surface, Desalination. 397 (2016) 38–42. doi:10.1016/j.desal.2016.06.022.

[10] K. Zeppenfeld, Electrochemical removal of calcium and magnesium ions from aqueous solutions, Desalination. 277 (2011) 99–105. doi:10.1016/j.desal.2011.04.005.

[11] D. Hasson, G. Sidorenko, R. Semiat, Calcium carbonate hardness removal by a novel electrochemical seeds system, Desalination. 263 (2010) 285–289. doi:10.1016/j.desal.2010.06.036.

[12] J.N. Apell, T.H. Boyer, Combined ion exchange treatment for removal of dissolved organic matter and hardness, Water Research. 44 (2010) 2419–2430. doi:10.1016/j.watres.2010.01.004.

[13] C. Gabrielli, G. Maurin, H. Francy-Chausson, P. Thery, T.T.M. Tran, M. Tlili, Electrochemical water softening: principle and application, Desalination. 201 (2006) 150–163.

[14] D. Hasson, H. Shemer, R. Semiat, Removal of scale-forming ions by a novel cation- exchange electrochemical system — A review, Desalination and Water Treatment. (2015) 1–15.

[15] S.L. Zhi, K.Q. Zhang, Hardness removal by a novel electrochemical method, Desalination. 381 (2016) 8–14. doi:10.1016/j.desal.2015.12.002.

[16] K. Rajeshwar, J.G. Ibanez, G.M. Swain, Electrochemistry and the environment, Journal of Applied Electrochemistry. 24 (1994) 1077–1091.

[17] D. Hasson, G. Sidorenko, R. Semiat, Low electrode area electrochemical scale removal system, Desalination and Water Treatment. 31 (2011) 35–41. http://www.tandfonline.com/doi/abs/10.5004/dwt.2011.2389.

[18] D. Hasson, V. Lumelsky, G. Greenberg, Y. Pinhas, R. Semiat, Development of the electrochemical scale removal technique for desalination applications, Desalination. 230 (2008) 329–342. doi:10.1016/j.desal.2008.01.004.

[19] J. Rinat, E. Korin, L. Soifer, A. Bettelheim, Electrocrystallization of calcium carbonate on carbon-based electrodes, Journal of Electroanalytical Chemistry. 575 (2005) 195–202. doi:10.1016/j.jelechem.2004.09.011.

[20] C. Gabrielli, G. Maurin, H. Perrot, G. Poindessous, R. Rosset, Investigation of electrochemical calcareous scaling Potentiostatic current- and mass- time transients, Journal of Electroanalytical Chemistry. 538–539 (2002) 133–143.

[21] R. Jaouhari, A. Benbachir, A. Guenbour, C. Gabrielli, J. Garcia-Jareno, G. Maurin, Influence of Water Composition and Substrate on Electrochemical Scaling, Journal of The Electrochemical Society. 147 (2000) 2151–2161. doi:10.1149/1.1393501.

[22] M. Dinamani, P.V. Kamath, R. Seshadri, Electrochemical synthesis of calcium carbonate coatings on stainless steel substrates, Materials Research Bulletin. 37 (2002) 661–669.

[23] L.. Simpson, Electrochemically generated CaCO3 deposits on iron studied with FTIR and Raman spectroscopy, Electrochimica Acta. 43 (1998) 2543–2547. doi:10.1016/S0013-4686(97)10167-0.

[24] L. Beaunier, C. Gabrielli, G. Poindessous, G. Maurin, R. Rosset, Investigation of electrochemical calcareous scaling Nuclei counting and morphology, Journal of Electroanalytical Chemistry. 501 (2001) 41–53.

[25] C. Gabrielli, G. Maurin, G. Poindessous, R. Rosset, Nucleation and growth of calcium carbonate by an electrochemical scaling process, Journal of Crystal Growth. 200 (1999) 236–250. doi:10.1016/S0022-0248(98)01261-5.

[26] I. Sanjuán, D. Benavente, V. García-García, E. Expósito, V. Montiel, Electrochemical softening of concentrates from an electrodialysis brackish water desalination plant: Efficiency enhancement using a three-dimensional cathode, Separation and Purification Technology. In press (2018) 0–10. doi:10.1016/j.seppur.2018.01.066.

[27] D. Hasson, A. Cornel, Effect of residence time on the degree of CaCO3 precipitation in the presence of an anti-scalant, Desalination. 401 (2017) 64–67. doi:10.1016/j.desal.2016.06.006.

[28] Donald Langmuir, Aqueous Environmental Geochemistry, 1997.

[29] D. Benavente, P. Brimblecombe, C.M. Grossi, Thermodynamic calculations for the salt crystallisation damage in porous built heritage using PHREEQC, Environmental Earth Sciences. 74 (2015) 2297–2313. doi:10.1007/s12665-015-4221-1.

[30] L. Fernández-Díaz, Á. Fernández-González, M. Prieto, The role of sulfate groups in controlling CaCO3polymorphism, Geochimica et Cosmochimica Acta. 74 (2010) 6064–6076. doi:10.1016/j.gca.2010.08.010.

[31] C. Deslouis, A. Doncescu, D. Festy, O. Gil, V. Maillot, S. Touzain, et al., Kinetics and Characterisation of Calcareous Deposits under Cathodic Protection in Natural Sea Water, Materials Science Forum. 289–292 (1998) 1163–1180. doi:10.4028/www.scientific.net/MSF.289-292.1163.

[32] F. Nindiyasari, E. Griesshaber, L. Fernández-Díaz, J.M. Astilleros, N. Sánchez-Pastor, A. Ziegler, et al., Effects of Mg and hydrogel solid content on the crystallization of calcium carbonate in biomimetic counter-diffusion systems, Crystal Growth and Design. 14 (2014) 4790–4802. doi:10.1021/cg500938k.

[33] J.M. Astilleros, L. Fernández-Díaz, A. Putnis, The role of magnesium in the growth of calcite: An AFM study, Chemical Geology. 271 (2010) 52–58. doi:10.1016/j.chemgeo.2009.12.011.

[34] J.S. Wey, P.H. Karpinski, Batch Crystallization, in: A.S. Myerson (Ed.), Handbook of Industrial Crystallization, Elsevier Inc., 2002: pp. 231–248.

[35] D. V. Okhrimenko, J. Nissenbaum, M.P. Andersson, M.H.M. Olsson, S.L.S. Stipp, Energies of the adsorption of functional groups to calcium carbonate polymorphs: The importance of -OH and -COOH groups, Langmuir. 29 (2013) 11062–11073. doi:10.1021/la402305x.

[36] M.M. Tlili, M. Benamor, C. Gabrielli, H. Perrot, B. Tribollet, Influence of the Interfacial pH on Electrochemical CaCO3 Precipitation, Journal of The Electrochemical Society. 150 (2003) C765–C771. doi:10.1149/1.1613294.

[37] C. Deslouis, I. Frateur, G. Maurin, B. Tribollet, Interfacial pH measurement during the reduction of dissolved oxygen in a submerged impinging jet cell, Journal of Applied Electrochemistry. 27 (1997) 482–492. doi:10.1023/A:1018430224622.

[38] J.O. Bockris, A.K.N. Reddy, Modern Electrochemistry. An introduction to an Interdisciplinary area. Volume 2., Plenum Publishing Corporation, 1970.

[39] I.M. Power, P.A. Kenward, G.M. Dipple, M. Raudsepp, Room Temperature Magnesite Precipitation, Crystal Growth and Design. 17 (2017) 5652–5659. doi:10.1021/acs.cgd.7b00311.

## Highlights

- Water composition has relevance on the electrochemical water softening efficiency.
- Ca is removed more efficiently than Mg by the electrochemical softening.
- Electroprecipitates has been fully characterised by SEM, XRD, TG and $N_2$ adsorption.
- Water composition strongly affects the properties of electroprecipitates.
- Geochemical calculations describe the electroprecipitation behaviour.

## Graphical Abstract